PLOS ONE

RESEARCH ARTICLE

Disturbance observer-based adaptive position control for a cutterhead anti-torque system

Hangjun Zhang[1], Jinhui Fang[1]*, Huan Yu[2], Huibin Hu[1], Yuzhu Yang[1]

1 State Key Laboratory of Fluid Power and Mechatronic Systems, Zhejiang University, Hangzhou, China,
2 Aerospace System Engineering Shanghai, Shanghai, China

* jhfang@126.com

Abstract

To conveniently replace worn cutterhead tools in complicated strata, a novel cutterhead attitude control mechanism was recently designed. Meanwhile, the mechanism also causes an engineering problem of how to control a matching cutterhead anti-torque system (CATS) effectively, which is used to prevent a drive box of the cutterhead from rotation during a complex excavation process. In this paper, a disturbance observer-based adaptive position controller is proposed for the CATS. The proposed method presents a nonlinear adaptive controller with adaptation laws to compensate for the unknown time-varying load torque and damping uncertainty in the system. Based on the disturbance observer method and sliding mode control, an asymptotically stable controller proven by Lyapunov theory is constructed using the back-stepping technique. In addition, a virtual test rig based on MATLAB and AMESim co-simulation is built to verify the validity of the proposed controller. The simulation results show that the proposed method has good performance for tracking tasks in the presence of uncertainties compared with PID control. Together, the data support targeting disturbance observer-based adaptive position control as a potential control strategy for cutterhead anti-torque systems.

1. Introduction

As an important carrier of underground transportation networks, tunnels have significant benefits in expanding urban space, relieving traffic congestion and exploiting natural resources. Tunnel boring machines are widely applied in tunnel construction since the shield tunnel method has distinct advantages over other methods in terms of efficiency, safety, environmental protection, etc. Among them, slurry shields are the preferred equipment for tunnel construction in high water pressure and high permeability sand strata [1–3]. To satisfy the growth of traffic demand, slurry shields have a trend toward upsizing, relying on the progress of shield construction technology. Meanwhile, large-diameter slurry shields face more challenges than normal shields in the construction process [4–7], such as excessive wear of the cutterhead and edge scrapers, instability of the tunnel face, complex attitude control of the heavy

cutterhead and difficult tunnel excavation in the upper-soft and lower-hard stratum. To address these problems, tunnel boring machine research institutions and manufacturers, including SKLOFP, Herrenknecht AG, CCCC and CRCHI, have successively designed and produced a new type of cutterhead attitude control mechanism [8–10], as shown in Fig 1. The cutterhead is connected to a drive box and driven by several inner electric or hydraulic motors. The drive box is fixed on an inner ring of a radial joint bearing whose outer ring is connected to a shield mechanism. A number of circular-distributed posture cylinders are installed on the backboard of the drive box, and the other sides are connected to a support seat of the shield mechanism. If these posture cylinders are extended or retracted synchronously, the cutterhead will move forward or backward. Therefore, an over-excavating specific soil space is constructed, which is used to replace the cutterhead worn tools or get out of shield jamming. The posture cylinders are different from the thrust cylinders used for forward digging in the whole excavation process. In addition, the inner motors drive the cutterhead to rotate through gears, and the cutterhead cuts the front soil and receives a reaction torque that drives the drive box to rotate radially. Due to the floating state of the drive box, a matching cutterhead anti-torque system (CATS) is designed to transmit the reaction torque to the shield structure and avoid
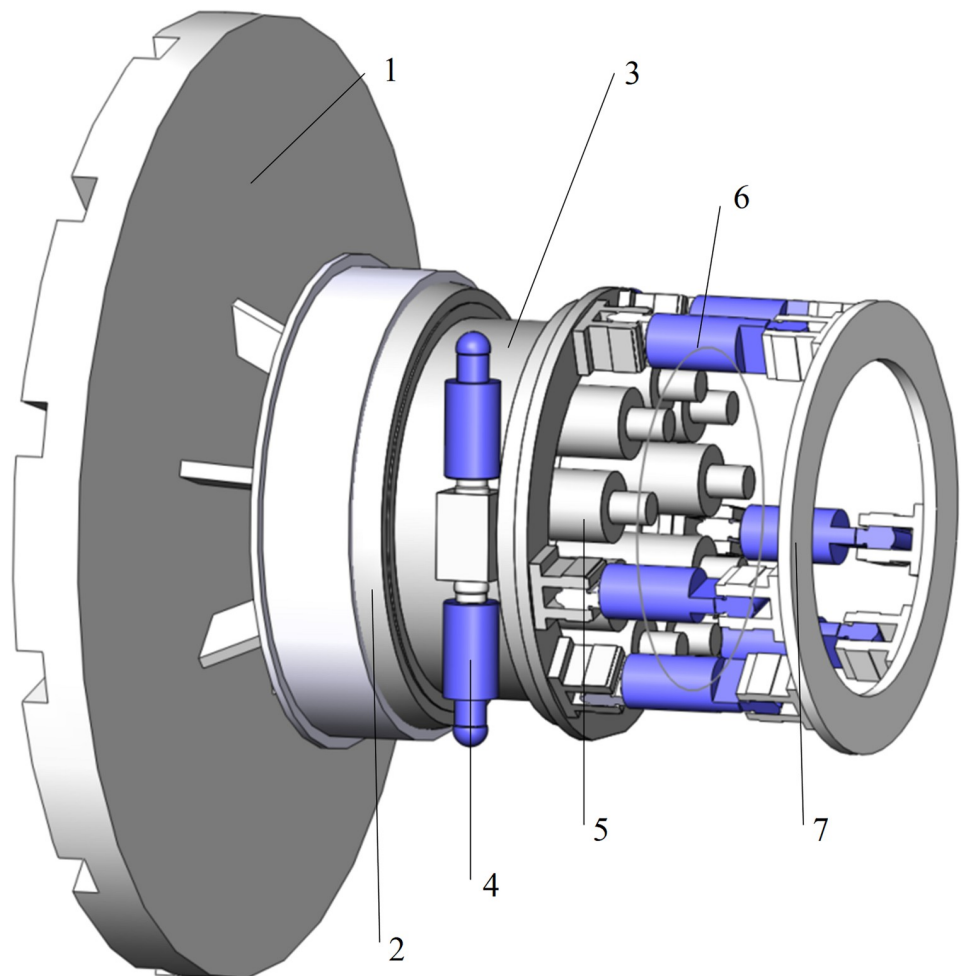

Fig 1. Cutterhead anti-torque system mechanism schematic. 1-Cutterhead, 2-Radial joint bearing, 3-Drive box, 4-Torque cylinder, 5-Motor, 6-Posture cylinder, 7-Support seat.

https://doi.org/10.1371/journal.pone.0268897.g001

drive box rotation against the shield. The main feature of the CATS is that two pairs of torque cylinders are equipped on both sides of the drive box symmetrically. The force of torque cylinders acts on the shield mechanism to provide reverse support and prevent the drive box from rotation during an excavation process.

The radial attitude of the drive box is controlled in real time by these torque cylinders driven by hydraulic power. Therefore, properly controlling the torque cylinders is the key technology to keep the drive box stable and improve tunnel construction efficiency and safety. PID control is currently the most mature and widely used control method in analog control systems, and it is also used in CATS control. However, hydraulic systems exhibit strong nonlinearities, such as nonlinear valve flow-pressure characteristics and temperature-varying oil properties. Hydraulic systems also have some model uncertainties, such as damping coefficients and unknown time-varying load forces. Both drawbacks cause control difficulties, in turn [11, 12]. Conventional PID controllers cannot achieve ideal control effects, and have poor adaptability to operating conditions. To obtain better dynamic performance, an increasing number of researchers have used nonlinear control strategies to compensate for nonlinearities and uncertainties. Under nominal operating conditions, the pole placement method [13] or adaptive control [14] was used to locally linearize the nonlinear dynamics. However, these controllers cannot provide excellent performance under all working conditions. The feedback linearization method [15], based on cancelling nonlinear terms, was used without taking system uncertainties into consideration. In addition, sliding mode control [16–19] has been widely used in hydraulic control systems. The dynamic behaviors on the sliding mode surface cannot be affected by model uncertainties and disturbances. However, the inherent chattering of the control input may cause high-frequency vibration and degrade the control performance. The concept of adaptive control [20, 21] was proposed in the research of autopilots of high-performance aircraft. This controller has a weak antidisturbance ability, although it is considered a valid method to overcome model uncertainties. The deterministic robust control method [22, 23] was applied to control nonlinear systems. In references [24, 25], Yao and Tomizuka developed adaptive robust control that effectively integrates adaptive control and deterministic robust control. They [26] applied a nonlinear adaptive robust controller for trajectory tracking of hydraulic actuators with uncertain nonlinearities and model uncertainties and achieved satisfying results. Furthermore, a desired compensation adaptive robust control framework [27] was also presented for nonlinear systems with uncertain nonlinearities and model uncertainties. In addition, many researchers applied a disturbance observer [28–31] to overcome the load disturbance and model uncertainties in complex systems, which had good trajectory tracking performance. Many observers provided an asymptotic or exponential convergence implying the error convergence to zero over an infinite time interval. In order to achieve a finite-time observation, several strategies have been presented and the sliding mode observer is one of the main methods with widespread applications. But the sliding mode observer is affected by some restrictions, leading to the potentially destructive chattering phenomenon in its convergence to zero. To eliminate the shortcoming, alternative approaches have been developed, such as the high-order sliding mode observer to reduce the chattering and the terminal sliding mode observer with finite-time convergence properties [32, 33]. Currently, to obtain better control performance, various nonlinear algorithms begin to be integrated [34–37], such as combining disturbance observer and sliding mode control, disturbance observer and adaptive control. Their experimental results showed the efficiency of novel nonlinear control strategy, although its structure was complex and difficult to be constructed. Besides, Chen and Zhu proposed a novel adaptive neural network observer in which the adaptive laws were constructed using quantized measurements. And accurate estimations of state and actuator efficiency factor can be obtained despite actuator degradation [38]. Zhu

also studies the observer-based output feedback control problem for a class of cyber-physical systems with periodic denial-of-service attacks. By means of a cyclic piecewise linear Lyapunov function approach, the observer-based controller design was carried out and its effectiveness was verified by unmanned ground vehicles under periodic denial-of-service attacks [39]. Slurry shields work in complicated strata, and the force with disturbance on the cutterhead is unknown and time-varying. Combined with the CATS control difficulties, to improve the accuracy and stability of the CATS in complicated strata, a disturbance observer-based adaptive position control strategy has been proposed. The proposed method presents a nonlinear adaptive controller with adaptation laws to compensate for the unknown time-varying load torque and damping uncertainty. The key feature of the control scheme is that by using the back-stepping technique, we combine the sliding mode control method and disturbance observer method to construct an asymptotically stable controller proven by Lyapunov theory. Simulation experiments are carried out by Simulink and AMESim co-simulation, and the results show the effectiveness of the proposed strategy in the presence of uncertainties.

The contributions of this paper are summarized as follow: first, a disturbance observer-based adaptive position control is successfully designed for CATS of slurry shields. As a result, more robust control performance can be achieved during experiments compared to the PID control. Second, the adaptation laws to compensate for the unknown time-varying load torque and damping uncertainty has shown to improve performance of the CATS. Third, the stability of proposed control is theoretically verified via a Lyapunov function analysis and the error is restricted within a certain range.

2. Dynamics model of CATS

The CATS includes four torque cylinders named as torque cylinders I, II, III and IV, as shown in Fig 2. One end of these cylinders is fixed on the drive box, and the other end is hinged to the shield structure. Torque cylinder I and II are equipped with a displacement sensor measuring its rod displacement, respectively. Since the rod-less chambers of the torque cylinder on the diagonal are connected to the same valve port through oil pipes, these cylinders have movement consistency. Their extending or retracting motions depend on the cutterhead sense of rotation. For example, the cutterhead cuts soil counterclockwise, the drive box receives a clockwise torque, torque cylinders I and IV are squeezed and torque cylinders II and III are stretched. In addition, the directional valve sets left way; torque cylinder I and IV are activated and controlled by a servo proportional valve, meanwhile torque cylinder II and III are still passive and maintained with 5 bar hydraulic pressure controlled by the relief valve, to ensure that the passive cylinders are slightly extended and in contact with the shield structure. If the stroke of torque cylinder II is larger than that of torque cylinder I, torque cylinders I and IV will be fed and extended. In contrast, torque cylinders I and IV will be released and retracted. In addition, the directional valve will set the right way if the cutterhead cuts soil clockwise. The torque cylinders can suppress the drive box rolling in real time and smoothly transmit the drive box torque to the shield structure.

For simplicity, take the cutterhead rotating counterclockwise as an example for mathematical model analysis. The directional valve sets left way and ignores the influence of the directional valve on the control system. In addition, the dynamics of the CATS can be given as

$$J\ddot{\varphi} = 2(P_1 - P_2)AL - (T + B\dot{\varphi})$$
$$x_l = L\varphi \tag{1}$$

where J is the equivalent moment of inertia of the drive box and cutterhead; φ is the roll angle of the drive box, $\dot{\varphi}$ and $\ddot{\varphi}$ are the angular velocity and acceleration, respectively; P_1 and P_2 are
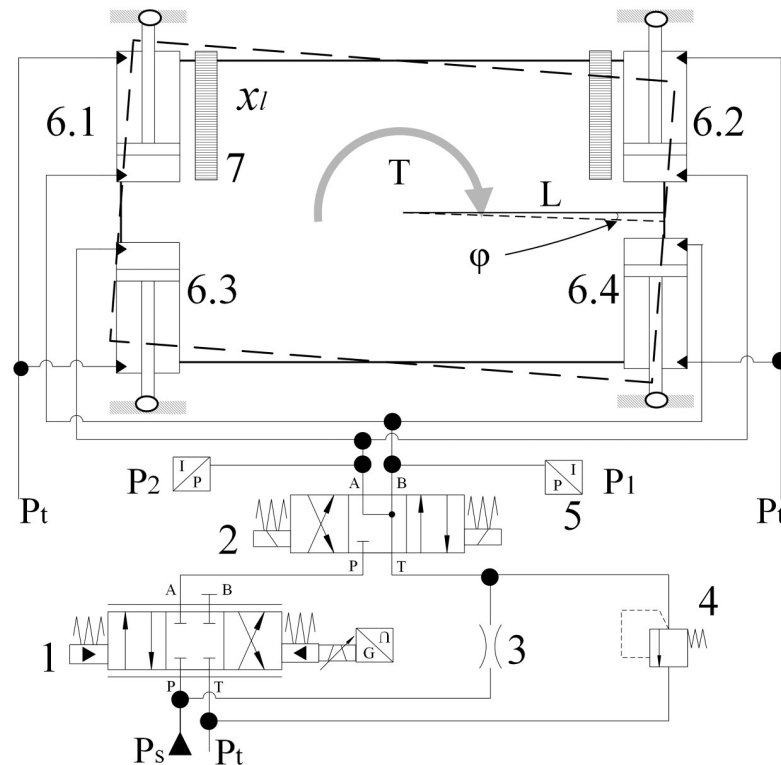
Fig 2. Schematic diagram of the hydraulic system. 1-Servo proportional valve, 2-Directional valve, 3-Fixed orifice, 4-Pressure relief valve, 5-Pressure sensor, 6.1-Torque cylinder I, 6.2 Torque cylinder II, 6.3-Torque cylinder III, 6.4-Torque cylinder IV, 7-Displacement sensor.

https://doi.org/10.1371/journal.pone.0268897.g002

the pressures in the active and passive cylinder rod-less chambers, respectively; A is the area of the cylinders rod-less side; L is the distance from the center of the drive box to the cylinder axis in the horizontal direction; T is the cutting anti-torque including some unknown disturbance; B is the combined coefficient of damping and viscous friction forces on the bearing, and x_l is the displacement of active torque cylinders. Here, we assume that the roll angle φ is very small due to the system working. The relationship between the roll angle φ and the active cylinder displacement x_l is linearized, and the drive box angle control can be converted into cylinder displacement control. The following simulation results show that the linearization is reliable in this situation. In addition, the passive torque cylinder displacement is defined as $-x_l$.

Considering the leakage and compressibility of the oil, the pressure dynamic of the active torque cylinder rod-less chamber can be written as

$$Q_1 = A\dot{x}_l + C_t P_1 + (V_0 + Ax_l)\beta_e^{-1}\dot{P}_1 \tag{2}$$

where Q_1 is the fluid flow rate of the active torque cylinder rod-less chamber; $\dot{x}_l$ is the velocity of active torque cylinders; C_t is the internal leakage coefficient; V_0 is the initial fluid volume of the active torque cylinder rod-less chamber; β_e is the bulk modulus of the fluid; and $\dot{P}_1$ is the derivative of pressure in the active cylinder rod-less chamber.

The fluid flow rate of the servo proportional valve Q is related to the spool displacement x_v and given as

$$Q = k_q x_v [\sigma(x_v)\sqrt{P_s - P_1} + \sigma(-x_v)\sqrt{P_1 - P_t}] \tag{3}$$

where the function $\sigma\,(^{*})$ is defined as

$$\sigma(*) = \begin{cases} 1 & if \quad * \quad \geq 0 \\ 0 & if \quad * \quad < 0 \end{cases} \tag{4}$$

k_q is the servo proportional valve flow gain coefficient; P_s is the source pressure, and P_t is the tank pressure. In addition, port B of the servo proportional valve connects two active torque cylinder rod-less chambers, thus Q and Q_1 have the following relationship.

$$Q = 2\,Q_1 \tag{5}$$

Since the dynamics of the servo proportional valve used here are much faster than others, the valve dynamics can be neglected, and the spool displacement is obtained [40] as follows:

$$x_v = k_v \cdot u \tag{6}$$

where k_v is a positive constant determined by valve design, and u is the control input voltage.

The state variables can be defined as $x = [x_1, x_2, x_3]^{\mathrm{T}} = [x_l, \dot{x}_l, P_1]^{\mathrm{T}}$. Including (1)–(6), the whole system can be expressed in a state-space form as follows:

$$\begin{aligned} \dot{x}_1 &= x_2 \\ \dot{x}_2 &= 2AL^2J^{-1}(x_3 - P_2) - LJ^{-1}T - BJ^{-1}x_2 \\ \dot{x}_3 &= h(x_1)^{-1}\left[-Ax_2 - C_t x_3 + \frac{k_q k_v R(x_3, u)}{2}u \right] \end{aligned} \tag{7}$$

where

$$\begin{aligned} R(x_3, u) &= \sigma(x_v)\sqrt{P_s - x_3} + \sigma(-x_v)\sqrt{x_3 - P_t} \\ h(x_1) &= (V_0 + Ax_1)\beta_e^{-1} \end{aligned} \tag{8}$$

Under normal conditions, P_1 and P_2 are bounded as $0 \leq P_t \leq P_1 \leq P_s$, $P_2 = 5$ bar.

3. Controller design

3.1 Disturbance observer

The disturbance observer we applied here is based on an extended state observer of x_2, although it is measurable. Thus, an additional degree of freedom for the controller is provided without the actuator acceleration signal. It can be described as

$$\dot{\hat{x}}_2 = 2AL^2J^{-1}(x_3 - P_2) - LJ^{-1}\hat{T} - x_2J^{-1}\hat{B} + \alpha\tilde{x}_2 \tag{9}$$

where $\hat{x}_2$, $\hat{T}$ and $\hat{B}$ are the estimations of x_2, T and B; $\dot{\hat{x}}_2$ is the derivative of $\hat{x}_2$. In addition, $\tilde{x}_2$ is the estimation error of x_2 and is defined as $\tilde{x}_2 = x_2 - \hat{x}_2$, and α is a positive feedback gain used to eliminate x_2 error. Including estimation errors $\tilde{T} = T - \hat{T}$ and $\tilde{B} = B - \hat{B}$, the dynamics of $\tilde{x}_2$ can be expressed as

$$\dot{\tilde{x}}_2 = -LJ^{-1}\tilde{T} - x_2J^{-1}\tilde{B} - \alpha\tilde{x}_2 \tag{10}$$

The adaptation law is chosen as

$$\begin{aligned} \dot{\hat{T}} &= Proj_{\hat{T}}(-\beta_1 LJ^{-1}\tilde{x}_2 + \gamma_1) \\ \dot{\hat{B}} &= -\beta_2 x_2 J^{-1}\tilde{x}_2 + \gamma_2 \end{aligned} \tag{11}$$

where β_1 and β_2 are positive constants; γ_1 and γ_2 are additional corrector parts designed to

ensure the stability of the whole system; $\dot{\hat{T}}$ and $\dot{\hat{B}}$ are the derivative of $\hat{T}$ and $\hat{B}$; and $Proj_{\hat{d}}(\cdot)$ is defined as

$$
Proj_{\hat{T}}(\bullet) = \begin{cases} 0 & if \quad \hat{T} = T_{\max} \quad and \quad \bullet > 0 \\[2mm] 0 & if \quad \hat{T} = T_{\min} \quad and \quad \bullet < 0 \\[2mm] \bullet & otherwise. \end{cases} \tag{12}
$$

And it can be found that $\hat{T} \in [T_{\min}, T_{\max}]$.

Define the following Lyapunov function V_1 as

$$
V_1 = \frac{1}{2}\tilde{x}_2^2 + \frac{1}{2}\beta_1^{-1}\tilde{T}^2 + \frac{1}{2}\beta_2^{-1}\tilde{B}^2 \tag{13}
$$

The time derivative of V_1 is given by

$$
\dot{V}_1 = -\alpha\tilde{x}_2^2 - \beta_1^{-1}\tilde{T}\gamma_1 - \beta_2^{-1}\tilde{B}\gamma_2 \tag{14}
$$

Remark 1: Since there is no more detailed information about the derivative of the load torque T and friction coefficient B, it is reasonable to assume that T and B vary slowly relative to the observer dynamics [41]; then, $\dot{T} \approx 0$ and $\dot{B} \approx 0$. The following simulation shows that the proposed controller is reliable in this situation.

3.2 Nonlinear position control

The nonlinear controller consists of a tracking control outer loop and a pressure control inner loop which provides the hydraulic actuator the characteristics of a force generator. Furthermore, sliding mode control is adopted to compensate for estimation errors. By using the recursive back-stepping technique, the controller is designed as follows.

Step 1: The goal of the step is to design a desired load force for the tracking control outer loop. This controller must be robust to estimation errors. Here, we define the tracking error as $\tilde{x}_1 = x_1 - x_d$, and $x_d = 0$. Then, a sliding mode surface s is defined as

$$
s = \dot{\tilde{x}}_1 + \lambda\tilde{x}_1 \tag{15}
$$

where λ is a positive constant. Making the tracking error small or converging to zero is the same as making s small or converging to zero, so the next process is to make s as small as possible.

From (15), the time derivative of s along system (7) is expressed as

$$
\dot{s} = 2AL^2J^{-1}(x_3 - P_2) - LJ^{-1}T - BJ^{-1}x_2 + \lambda x_2 \tag{16}
$$

In the pressure control inner loop, design a virtual controller y_3 for x_3 as

$$
y_3 = P_2 + [LJ^{-1}\hat{T} + x_2J^{-1}\hat{B} - \lambda x_2 - \eta_1 s]J/(2AL^2) \tag{17}
$$

where η_1 is a positive constant used to eliminate pressure tracking error. Here, we define the tracking error of the pressure control inner loop as $z_3 = x3 - y_3$. Combining (16) and (17), we can obtain

$$
\dot{s} = -LJ^{-1}\tilde{T} - x_2J^{-1}\tilde{B} - \eta_1 s + 2AL^2J^{-1}z_3 \tag{18}
$$

Define the following Lyapunov function V_2 as

$$V_2 = V_1 + \frac{1}{2}\beta_3^{-1}s^2 \tag{19}$$

where β_3 is a positive constant.

The time derivative of V_2 is given by

$$\dot{V}_2 = -\alpha\tilde{x}_2^2 - (\beta_1^{-1}\gamma_1 + Ls\beta_3^{-1}J^{-1})\tilde{T} - (\beta_2^{-1}\gamma_2 + x_2s\beta_3^{-1}J^{-1})\tilde{B} - \beta_3^{-1}\eta_1 s^2 + \beta_3^{-1}2AL^2J^{-1}z_3 s \tag{20}$$

Then, the additional corrector parts mentioned before are chosen as

$$\begin{aligned} \gamma_1 &= -Ls\beta_3^{-1}J^{-1}\beta_1 \\ \gamma_2 &= -x_2 s\beta_3^{-1}J^{-1}\beta_2 \end{aligned} \tag{21}$$

Substitute (21) into (20), and we can get

$$\dot{V}_2 = -\alpha\tilde{x}_2^2 - \beta_3^{-1}\eta_1 s^2 + 2AL^2J^{-1}z_3 s\beta_3^{-1} \tag{22}$$

Step 2: In step 1, we have designed a virtual control law y_3 which is the command input of the inner load pressure control loop. In this step, an actual control law for u is determined.

From (7), the time derivative of z_3 is given by

$$\dot{z}_3 = h(x_1)^{-1}\left[-Ax_2 - C_t x_3 + \frac{k_q k_v R(x_3, u)}{2}u\right] - \dot{y}_3 \tag{23}$$

And the actual control u is designed as

$$\begin{aligned} u &= \frac{2u_x}{k_q k_v R(x_3, u)} \\ u_x &= Ax_2 + C_t x_3 + h(x_1)(\dot{y}_3 - \eta_2 z_3 - \beta_3^{-1}\beta_4 2AL^2J^{-1}s) \end{aligned} \tag{24}$$

where η_2 and β_4 are both positive constants.

Remark 2: Note that (24) includes the control input u on both sides of the equation, so (24) cannot be calculated directly. However, the control input u on the right side is only used for $R(\cdot)$, since $R(\cdot)$ is always greater than zero, the sign of u is determined by u_x.

Substitute (24) into (23), and we can get

$$\dot{z}_3 = -\eta_2 z_3 - \beta_3^{-1}\beta_4 2AL^2J^{-1}s \tag{25}$$

Define the following Lyapunov function V_3 as

$$V_3 = V_2 + \frac{1}{2}\beta_4^{-1}z_3^2 \tag{26}$$

From (26), the time derivative of V_3 is given by

$$\dot{V}_3 = -\alpha\tilde{x}_2^2 - \beta_3^{-1}\eta_1 s^2 - \beta_4^{-1}\eta_2 z_3^2 \tag{27}$$

It is obvious that $\dot{V}_3 \leq 0$. The stability of the closed-loop system is guaranteed by Lyapunov theory, and all system signals are bounded under closed-loop control.

Theorem 1: Lyapunov's second method for stability makes use of a Lyapunov function $V(x)$ which has an analogy to the potential function of classical dynamics. It is introduced as follows for a system $\dot{x} = f(x)$ having a point of equilibrium at $x = 0$. Consider a function $V: R^n \rightarrow R$
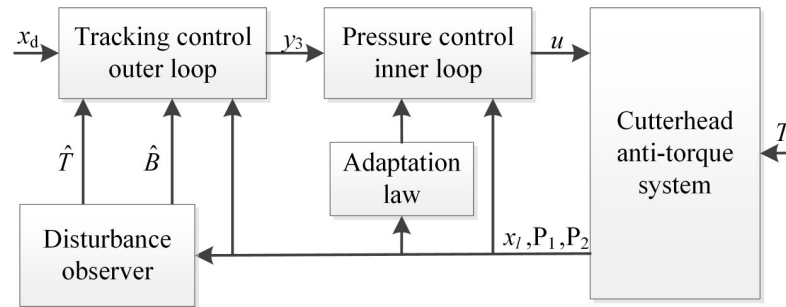
Fig 3. Block diagram of the controller structure.

such that

$$V(x) = 0 \; if \; and \; only \; if \; x = 0;$$

$$V(x) > 0 \; if \; and \; only \; if \; x \neq 0;$$

$$\dot{V}(x) = \frac{d}{dt} V(x) = \nabla V \cdot f(x) = \sum_{i=1}^{n} \frac{\partial V}{\partial x_i} f_i(x) \leq 0 \; for \; all \; values \; of \; x \neq 0.$$

Then $V(\mathrm{x})$ is called a Lyapunov function and the system is stable in the sense of Lyapunov. The block diagram of the adaptive controller structure is shown in Fig 3.

4. Simulation results

To test the proposed disturbance observer-based adaptive position control, simulations are performed using the MATLAB and AMESim co-simulation method. The virtual test rig shown in Fig 4 is mainly composed of 4 torque cylinders, 2 load cylinders and their matching electrohydraulic system. And dimensions of the torque cylinders are 600mm/520mm/400mm. The servo proportional valve used is the 4WRPH6C4B40L-type valve made by Rexroth, and the control input is [−10,10] V. The mechanism structure and size are close to those of a fifteen-meter-diameter slurry shield numbered S-1046 produced by Herrenknecht Ag. Torque cylinders can be controlled by one servo proportional valve, and then the attitude of the drive box can be adjusted precisely. In addition, the force of the load cylinders can be set to simulate the load torque and cause a rotation of the drive box.

To verify the performance of the adaptive position controller, the external load force F is set as shown below:

$$F = \begin{cases} (2 - 2\cos(\pi t)) * 10^5 \quad N \quad & if \; t \; < 1s \\ (7 - 3\sin(0.5\pi t)) * 10^5 \; N \quad & else \end{cases} \tag{28}$$

In addition, disturbance is unknown, and x_d is 0. The parameters of CATS and controller are chosen according to Tables 1 and 2. And the proposed control parameters are well tuned.

Traditional PID control is compared with the proposed control in this paper. And the input control u of PID control is given by

$$u = 2000(x_d - x_1) + 500 \int_0^t (x_d - x_1) d_t + 100 \frac{d(x_d - x_1)}{d_t} \tag{29}$$

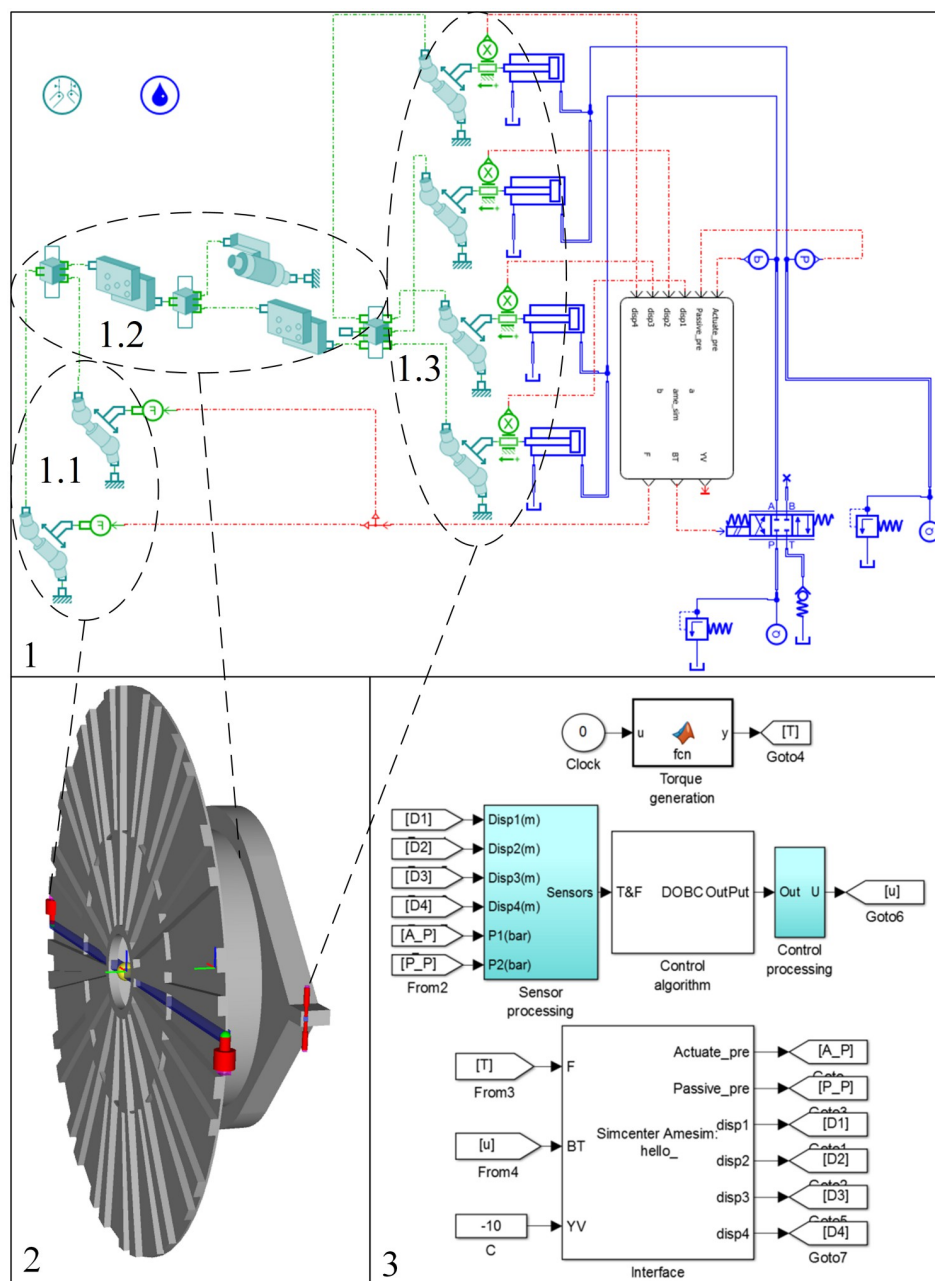The PID control algorithm parameters are well tuned and used in the whole process.

Fig 4. Virtual test rig of the CATS. 1-AMESim simulation model of the CATS, 1.1-Load cylinder, 1.2-Mechanism, 1.3-Torque cylinder, 2-Virtual 3D structure built by AMESim, 3-MATLAB control algorithm.

The desired displacement of the torque cylinders is shown as a black line in Fig 5a. The two controllers drive each torque cylinder to track its desired displacement as closely as possible to prevent the drive box from rotation. The red line and blue line present the tracking performance of the proposed method and PID method, respectively. The proposed controller performs better than the PID controller in terms of position tracking error. The tracking error of the PID method is more than twice that of the proposed method which is bounded within ±0.13 mm. At the beginning, the cutterhead anti-torque system with the proposed controller

Table 1. The parameters of CATS.

Parameter	Description	Value
J	Moment of inertia of the drive box and cutterhead	$2.45 * 10^6$ kg·m^2
A	Cylinder chamber area	0.283 m^2
V_0	Cylinder chamber initial volume	$5.66 * 10^{-2}$ m^3
L	Distance from the center of the drive box to the cylinder axis	5.00 m
P_s	Source pressure	$2.50 * 10^7$ Pa
P_t	Tank pressure	0 Pa
$K_q \cdot K_v$	Valve flow gain coefficient	$1.43 * 10^{-7}$ m^3/(s · V · $\sqrt{Pa}$)
β_e	Oil bulk modulus	$1.00 * 10^9$ Pa
C_t	Cylinder leakage coefficient	$1.00 * 10^{-14}$ m^3/(s·Pa)

Table 2. The parameters of proposed controller.

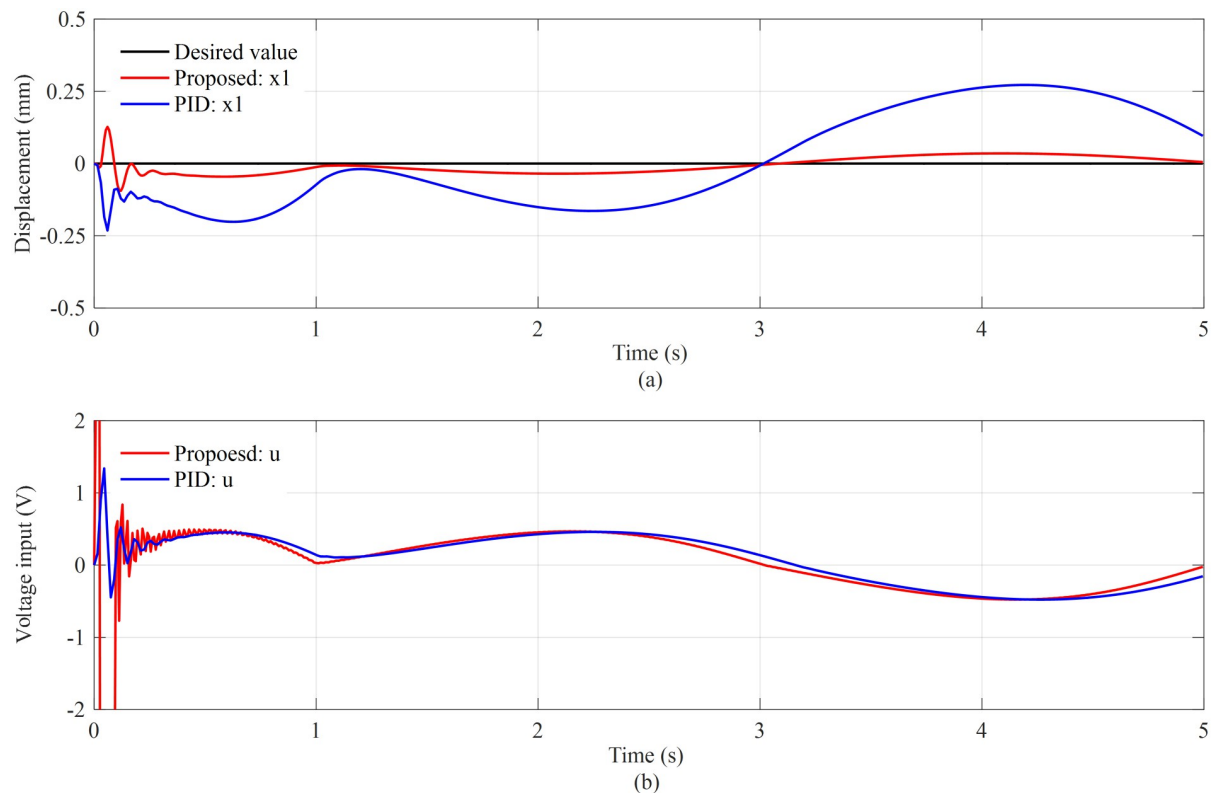| Parameter	Value	Parameter	Value
β_1	$1.25 * 10^{12}$	η_2	12
β_2	$1.25 * 10^{12}$	α	2000
β_3	0.001	λ	250
β_4	0.01	$\hat{T}(0)$	0
η_1	120	$\hat{B}(0)$	0

Fig 5. Tracking performance (a) and control input voltages (b) of the two controller methods.

cannot follow the desired trajectory smoothly due to the difference between the initial and desired system states. However, after 0.3 seconds of adjustment, the displacement of the torque cylinders is appropriately controlled and bounded within ±0.05 mm. It can be considered that the torque cylinders are well controlled during the entire stroke process. The control input voltages of servo proportional valves are shown in Fig 5b. Without considering the adjusted state, the control input values are reasonable, laying the foundation for smooth responses of the torque cylinders.

Moreover, the error of sliding surface s shown in Fig 6a is also bounded within ±0.04, and after its adjustment, the error is constrained within ±0.01, indicating that, similar to the displacement, the velocity of torque cylinders is well controlled, and their tracking errors are small. This shows that the tracking control outer loop performs well. Fig 6b shows that the nominal controller y_3 tracks the desired x_3 value, and the maximum error that appears at the beginning is less than 10 bar. After its adjustment, the error is bounded within ±5 bar. Thus, it can be considered that the pressure control inner loop performs well.

Fig 7a shows the velocity estimation of torque cylinders based on the disturbance observer. The estimation of velocity is relatively close to the actual velocity. In addition, the estimation error is bounded within ±3 mm/s. Fig 7b presents the torque estimation and the friction coefficient estimation based on the adaptation law. The trend of torque estimation is similar to that of load force, and the estimation of the combined friction coefficient is stable at approximately -1100. Since the displacement and pressure track well, it can be considered that the torque and the friction coefficient are estimated well.
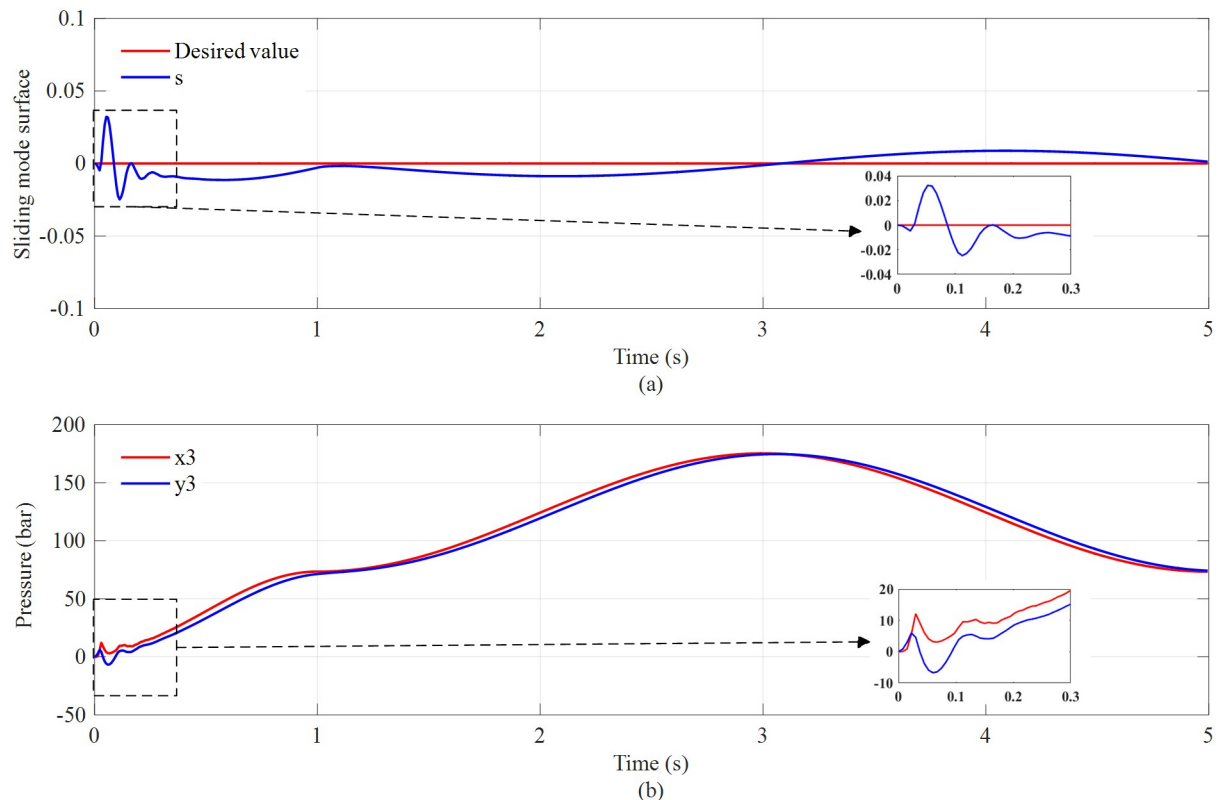

Fig 6. Sliding mode surface (a) and pressure in the rodless chamber of the active torque cylinder (b).
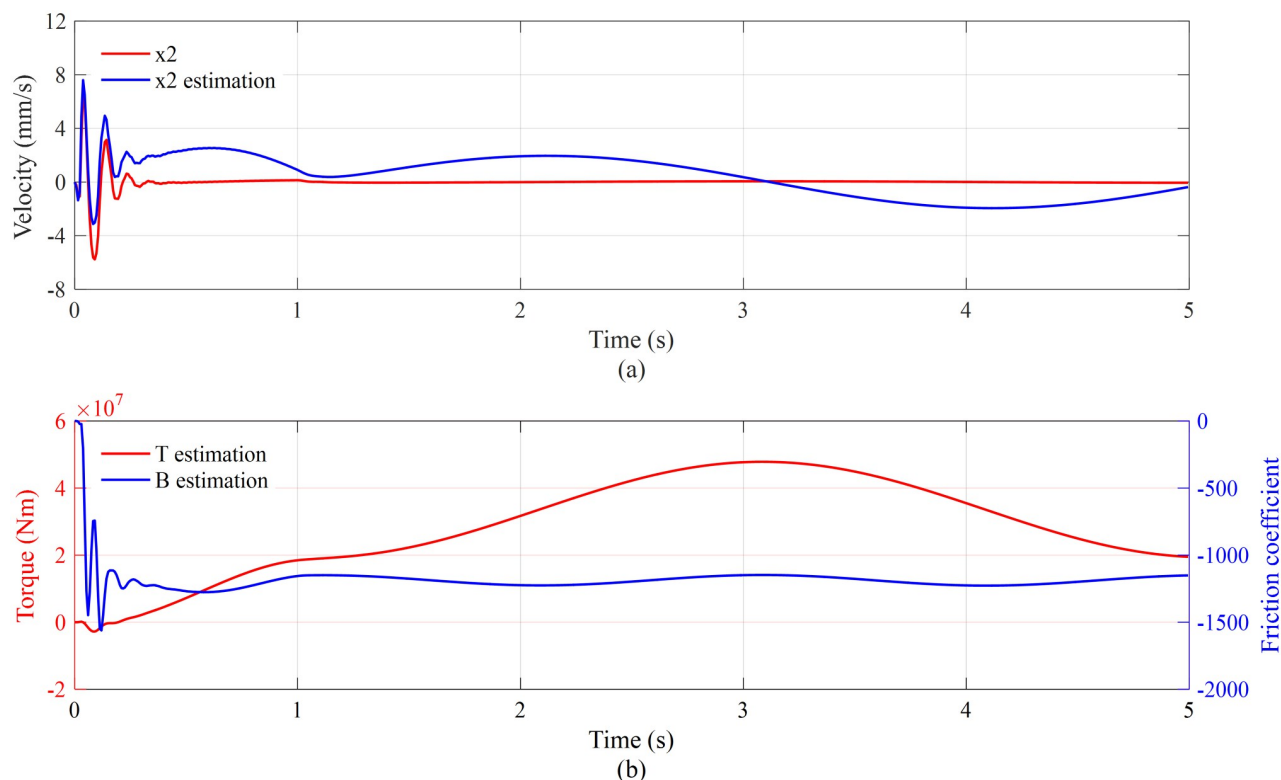
Fig 7. Velocity estimation (a) and torque and friction coefficient estimation (b).

Above all, the simulation results prove strongly that the proposed controller has good performance and great control accuracy in the presence of uncertainties.

5. Conclusion

In this work, disturbance observer-based adaptive position control for a cutterhead anti-torque system is proposed. The proposed method presents a nonlinear adaptive controller with adaptation laws to compensate for the unknown time-varying load torque and damping uncertainty. By using the back-stepping technique, an asymptotically stable controller proven by Lyapunov theory is constructed based on the disturbance observer method and sliding mode control. In addition, the validity of the proposed controller is verified by MATLAB and AME-Sim co- simulation. The simulation results show good performance for the tracking task in the presence of uncertainties compared with the traditional PID strategy. Together, the data support targeting disturbance observer-based adaptive position control as a potential control strategy for cutterhead anti-torque systems.

Supporting information

S1 Data.
(ZIP)

Author Contributions

Data curation: Hangjun Zhang, Huibin Hu, Yuzhu Yang.

Investigation: Hangjun Zhang, Huan Yu, Yuzhu Yang.

Methodology: Hangjun Zhang, Huan Yu.

Project administration: Jinhui Fang.

Software: Hangjun Zhang, Huan Yu.

Writing – original draft: Hangjun Zhang.

Writing – review & editing: Hangjun Zhang, Jinhui Fang.

References

1. Wang LT, Yang X, Gong GF, Du JN. Pose and trajectory control of shield tunneling machine in complicated stratum. Automation in Construction. 2018; 93:192–9. https://doi.org/10.1016/j.autcon.2018.05.020

2. Wang SM, Lu XX, Wang XM, He C, Xia X, Ruan L, et al. Soil improvement of EPBS construction in high water pressure and high permeability sand stratum. Advances in Civil Engineering. 2019; 2019:1–9. https://doi.org/10.1155/2019/4503219

3. Li XF, Gong GF. Predictive control of slurry pressure balance in shield tunneling using diagonal recurrent neural network and evolved particle swarm optimization. Automation in Construction. 2019; 107. https://doi.org/10.1016/j.autcon.2019.102928

4. Li XG, Yuan DJ. Creating a working space for modifying and maintaining the cutterhead of a large-diameter slurry shield: A case study of Beijing railway tunnel construction. Tunnelling and Underground Space Technology. 2018; 72:73–83. https://doi.org/10.1016/j.tust.2017.11.008

5. He XC, Xu YS, Shen SL, Zhou AN. Geological environment problems during metro shield tunnelling in Shenzhen, China. Arabian Journal of Geosciences. 2020; 13(2). https://doi.org/10.1007/s12517-020-5071-z

6. Zhang F, Gao YF, Wu YX, Wang ZX. Face stability analysis of large-diameter slurry shield-driven tunnels with linearly increasing undrained strength. Tunnelling and Underground Space Technology. 2018; 78:178–87. https://doi.org/10.1016/j.tust.2018.04.018

7. Yang SQ, Chen M, Fang G, Wang YC, Meng B, Li YH, et al. Physical experiment and numerical modelling of tunnel excavation in slanted upper-soft and lower-hard strata. Tunnelling and Underground Space Technology. 2018; 82:248–64. https://doi.org/10.1016/j.tust.2018.08.049

8. Yao ZH, Yang Z, Tian Y, Hu HT. Key construction technology for the Nanjing Weisan Road River-Crossing Tunnel Project. Modern Tunnelling Technology. 2015; 52(04):15–23. https://doi.org/10.13807/j.cnki.mtt.2015.04.003

9. Tan SH, Sun H. Key design technologies for cutter replacing of super-large slurry shield under atmaspheric condition: Case studies of Shantou Gulf Tunnel and Shenzhen Chunfeng Tunnel. Tunnel Construction. 2019; 39(07):1073–82. https://doi.org/10.3937/j.issn.2096-4498.2019.07.001

10. Herrenknecht EhM, Bäppler K. Mastering risks during mechanized excavation in urban centers with highly complex ground conditions. Tunnelling and Underground Space Technology. 2006; 21(3):260. https://doi.org/10.1016/j.tust.2005.12.121

11. Guo K, Wei JH, Fang JH, Feng RL, Wang XC. Position tracking control of electro-hydraulic single-rod actuator based on an extended disturbance observer. Mechatronics. 2015; 27:47–56. https://doi.org/10.1016/j.mechatronics.2015.02.003

12. Maier CC, Schröders S, Ebner W, Köster M, Fidlin A, Hametner C. Modeling and nonlinear parameter identification for hydraulic servo-systems with switching properties. Mechatronics. 2019; 61:83–95. https://doi.org/10.1016/j.mechatronics.2019.05.005

13. Plummer A.R., Vaughan N.D. Decoupling pole-placement control, with application to a multi-channel electro-hydraulic servosystem. Control Engineering Practice. 1997; 5(3):313–23. https://doi.org/10.1016/S0967-0661(97)00008-7

14. Tan KK, Lee TH, Huang SN. Adaptive control of ram velocity for the injection moulding machine. IFAC Proceedings Volumes. 1999; 32(2):6854–9. https://doi.org/10.1016/s1474-6670(17)57170-0

15. Seo J, Venugopal R, Kenné JP. Feedback linearization based control of a rotational hydraulic drive. Control Engineering Practice. 2007; 15(12):1495–507. https://doi.org/10.1016/j.conengprac.2007.02.009

16. Guan C, Pan SX. Adaptive sliding mode control of electro-hydraulic system with nonlinear unknown parameters. Control Engineering Practice. 2008; 16(11):1275–84. https://doi.org/10.1016/j.conengprac.2008.02.002

17. Shen W, Wang JH. An integral terminal sliding mode control scheme for speed control system using a double-variable hydraulic transformer. ISA Trans. 2019. https://doi.org/10.1016/j.isatra.2019.08.068 PMID: 31648794

18. Dang XJ, Zhao XA, Dang C, Jiang H, Wu XR, Zha LT. Incomplete differentiation-based improved adaptive backstepping integral sliding mode control for position control of hydraulic system. ISA Trans. 2021; 109:199–217. https://doi.org/10.1016/j.isatra.2020.10.027 PMID: 33059903

19. Schmidt L, Andersen TO, Pedersen HC. Robust non-chattering observer based sliding control concept for electro-hydraulic drives. IFAC Proceedings Volumes. 2013; 46(5):99–108. https://doi.org/10.3182/20130410-3-cn-2034.00041

20. Jhan FH, Lin JS. Nonlinear and adaptive control design of a helicopter in vertical flight. 2011 8th Asian Control Conference (ASCC); 2011: IEEE Computer Society.

21. Shin J, Kim HJ, Kim Y, Tahk M. Adaptive control using support vector regression for hypersonic aircraft control system. Proc Int Council Aeronaut Sci Congr; 2010.

22. Freeman RA, Kokotovic PV. Design of 'softer' robust nonlinear control laws. Automatica. 1993; 29 (6):1425–37. https://doi.org/10.1016/0005-1098(93)90007-G

23. Liu JF, Abdel Malek K. Robust control of planar dual-arm cooperative manipulators. Robotics and Computer-Integrated Manufacturing. 2000; 16(2):109–19. https://doi.org/10.1016/S0736-5845(99)00043-5

24. Yao B, Tomizuka M. Smooth robust adaptive sliding mode control of manipulators with guaranteed transient performance. Journal of Dynamic Systems, Measurement, and Control, Transactions of the ASME. 1996; 118(4):764–75. https://doi.org/10.1115/1.2802355

25. Yao B, Tomizuka M. Adaptive robust control of SISO nonlinear systems in a semi-strict feedback form. Automatica. 1997; 33(5):893–900. https://doi.org/10.1016/S0005-1098(96)00222-1

26. Yao B, Bu FP, Reedy J, Chiu GTC. Adaptive robust motion control of single-rod hydraulic actuators: Theory and experiments. IEEE/ASME Transactions on Mechatronics. 2000; 5(1):79–91. https://doi.org/10.1109/3516.828592

27. Yao B, Kuang P. Desired compensation adaptive robust control. Journal of Dynamic Systems, Measurement and Control, Transactions of the ASME. 2009; 131(6):1–7. https://doi.org/10.1115/1.3211087

28. Chen WH. Disturbance observer based control for nonlinear systems. IEEE/ASME Transactions on Mechatronics. 2004; 9(4):706–10. https://doi.org/10.1109/TMECH.2004.839034

29. Kim W, Shin D, Won D, Chung CC. Disturbance-observer-based position tracking controller in the presence of biased sinusoidal disturbance for electrohydraulic actuators. IEEE Transactions on Control Systems Technology. 2013; 21(6):2290–8. https://doi.org/10.1109/TCST.2013.2237909

30. Pi YJ, Wang XY. Observer-based cascade control of a 6-DOF parallel hydraulic manipulator in joint space coordinate. Mechatronics. 2010; 20(6):648–55. https://doi.org/10.1016/j.mechatronics.2010.07.002

31. Wei JH, Zhang Q, Li MJ, Shi WZ. High-performance motion control of the hydraulic press based on an extended fuzzy disturbance observer. Proceedings of the Institution of Mechanical Engineers, Part I: Journal of Systems and Control Engineering. 2016; 230(9):1044–61. https://doi.org/10.1177/0959651816662562

32. Palli G, Strano S, Terzo M. Sliding-mode observers for state and disturbance estimation in electro-hydraulic systems. Control Engineering Practice. 2018; 74:58–70. https://doi.org/10.1016/j.conengprac.2018.02.007

33. Wang B, Shao YZ, Yu Y, Dong QH, Yun ZP, Xu DG. High-order terminal sliding-mode observer for chattering suppression and finite-time convergence in sensorless SPMSM drives. IEEE Transactions on Power Electronics. 2021; 36(10):11910–20. https://doi.org/10.1109/TPEL.2021.3068495

34. Koch S, Reichhartinger M. Observer-based sliding mode control of hydraulic cylinders in the presence of unknown load forces. Elektrotechnik und Informationstechnik. 2016; 133(6):253–60. https://doi.org/10.1007/s00502-016-0418-6

35. Kim JG, Han CH, Jeong SK. Disturbance observer-based robust control against model uncertainty and disturbance for a variable speed refrigeration system. International Journal of Refrigeration. 2020; 116:49–58. https://doi.org/10.1016/j.ijrefrig.2020.03.019

36. Li M, Chen Y, Liu YZ. Adaptive disturbance observer-based event-triggered fuzzy control for nonlinear system. Information Sciences. 2021; 575:485–98. https://doi.org/10.1016/j.ins.2021.06.055

37. Wang JB, Liu L, Liu CX. Sliding mode control with mismatched disturbance observer for chaotic oscillation in aseven-dimensionalpower system model. International Transactions on Electrical Energy Systems. 2020; 30(11). https://doi.org/10.1002/2050-7038.12583

38. Chen LH, Zhu YZ, Ahn CK. Adaptive neural network-based observer design for switched systems with quantized measurements. IEEE transactions on neural networks and learning systems. 2021. https://doi.org/10.1109/TNNLS.2021.3131412 PMID: 34890344

39. Zhu YZ, Zheng WX. Observer-based control for cyber-physical systems with periodic DoS attacks via a cyclic switching strategy. IEEE Transactions on Automatic Control. 2020; 65(8):3714–21. https://doi.org/10.1109/TAC.2019.2953210

40. Sohl GA, Bobrow JE. Experiments and simulations on the nonlinear control of a hydraulic servosystem. IEEE Transactions on Control Systems Technology. 1999; 7(2):238–47. https://doi.org/10.1109/87.748150

41. Chen WH, Ballance DJ, Gawthrop PJ, Reilly JO. A nonlinear disturbance observer for robotic manipulators. IEEE Transactions on Industrial Electronics. 2000; 47(4):932–8. https://doi.org/10.1109/41.857974